PHILOSOPHICAL TRANSACTIONS OF THE ROYAL SOCIETY A MATHEMATICAL, PHYSICAL & ENGINEERING SCIENCES

Turbulent Suspension of Sediments in the Deep Sea

T. F. Gross and A. R. M. Nowell

Phil. Trans. R. Soc. Lond. A 1990 **331**, 167-181
doi: 10.1098/rsta.1990.0063

Phil. Trans. R. Soc. Lond. A **331**, 167–181 (1990) [167]
Printed in Great Britain

Turbulent suspension of sediments in the deep sea

By T. F. Gross[1] and A. R. M. Nowell[2]

[1] *Skidaway Institute of Oceanography, P.O.* 13687, *Savannah, Georgia* 31416, *U.S.A.*
[2] *School of Oceanography, University of Washington, Seattle, Washington* 98195, *U.S.A.*

The high-energy benthic boundary layer experiment demonstrated the existence of high energy events capable of suspending large amounts of sediment at the base of the Nova Scotian Rise. The currents that cause these storms are episodic pulses of 25–35 cm s^{-1} flows lasting four to seven days. The build up and decay of the currents is too rapid for local equilibrium of the suspended sediment distribution to be achieved. Therefore, a fully time-dependent model of the turbulent boundary layer and the suspended sediments was developed to describe the events in detail.

The period of high flow is erosive for only a few hours. The surface erodible bed sediments are quickly removed. The dominant processes resulting in the development of the suspended sediment profile are then restricted to turbulent diffusion and entrainment. The depth of penetration of the suspended sediments into the water column is limited by stratification induced by suspended sediments. After the shear generated turbulence collapses most of the eroded sediment remained in suspension far above the expected 'equilibrium' height for a 'non-storm' turbulent boundary layer. Scaling arguments, and the model, show that fine clay particles kept in suspension by turbulent diffusion dominate settling during the low level turbulence present during 'non-storm' conditions. Level 2 and $2\frac{1}{2}$ energy closure models with stratification predict quite different structures of the nepheloid layer.

Introduction

High-energy deep-sea currents are believed to be responsible for large concentrations of suspended sediment observed in nepheloid layers (Hollister & McCave 1984). Large temporal and spatial variability of the near-bed suspended sediment load results from the advection of clouds of sediment suspended by localized and short duration events. Most of the 'storms' observed during the high-energy benthic boundary layer experiment (HEBBLE) were of this advected type (Gross & Williams 1990). However, several erosion events, local storms, were observed (Gross *et al.* 1988). During the HEBBLE year-long deployments, two of the fourteen significant suspended sediment events were local storms (Gross & Williams 1990). A model of the dynamics of erosion events is developed to demonstrate the magnitude, structure and behaviour of both advected clouds and local storms. The signature of a local storm is recreated with a time-dependent model of the suspended sediment field based entirely on assumptions of local dynamics.

The depth and growth of the near-bed turbulence supported nepheloid layer depends on the structure and thickness of the benthic boundary layer. Most turbulence closure methods are similar in the logarithmic region near the bed. Unfortunately there are large differences between closure models in the outer layer where entrainment dominates the growth of the nepheloid layer. Several closure models are discussed and their applicability to benthic sediment transport storms is evaluated.

Models of the suspended sediment profile must include the effects of stratification, variability of sediment concentration and size distribution in the source bed, and temporal variability in the turbulent forcing of the bottom boundary layer. Although the suspended sediment loads during HEBBLE were relatively small the outer layer dynamics will be affected by sediment induced stratification. Near the bed, where shear induced turbulence is large, stratification can be safely ignored. However, there must be a point above the logarithmic region where sediment stratification will control the production of turbulent kinetic energy. Depth and intensity of the sediment induced pycnocline is a function of the strength and duration of the bottom stresses and the total load of sediment suspended. Closure models based on the kinetic energy equation are used to demonstrate this effect.

Observations during HEBBLE

The HEBBLE was designed to test the hypothesis that relatively infrequent high-energy flow events capable of suspending large amounts of sediments occur along the Nova Scotian Rise (Nowell *et al.* 1982). Whether such events are frequent and of long enough duration to suspend an appreciable fraction of particles making up the nepheloid layer was tested during a year long (September 1985 to September 1986) deployment of instruments. The principle instrument used for monitoring the bottom boundary layer currents, turbulent stress and energy were the benthic acoustic stress sensors (BASS) (Williams *et al.* 1987; Gross *et al.* 1986; Gross & Williams 1990). The BASS are arrayed on a stationary tripod at heights above bottom of 47, 82, 219 and 495 cm. Light transmissometers were used to measure suspended sediment concentration.

The HEBBLE site is situated on the Nova Scotian Rise (40° 26.5′ N, 62° 21.7′ W), an area that is frequently swept by westward along isobath bottom currents. This area was chosen because of its simple, smooth topography. The surface sediments are composed of consolidated silt and clays extensively reworked by epibenthic fauna (Thistle *et al.* 1985). There was considerable variability in the western flow on all timescales, including M_2 internal tidal energy. Maximum currents are up to 30 cm s^{-1} at 5 metres above bottom (m AB) and are usually west to southwestward.

Measures of turbulent energy and stress generally tracked the velocity. However, considerable variability in bottom drag coefficient or bed roughness (z_o) occurs (Gross *et al.* 1986). Photographs of the sea bed indicate that modification of the sea bed by currents and biological activity is common, and may account for the temporal variability of z_o. Active sediment transport and stratification are also expected to affect logarithmic profile estimates of z_o and drag coefficients.

Suspended sediment concentrations are not simply related to current magnitude. Of the possible 14 suspended sediment events only two, on October 24 and June 15, seem to be due to local erosion (figs 1, 2 and 3 of Gross & Williams 1990). Most events resulted from the advection of suspended sediment into the area. Figure 1 depicts three events of high suspended load, which appear associated with changes in direction of the current, and not with strong currents and bed stresses. An inverted progressive vector diagram of the period November 10 to November 15, with concentration marked along the path, is presented in figure 2. A sediment concentration field with gradients up to 200 μg dm^{-3} km^{-1} moved into the area from the north and returned to the north several days later. The repeatability of the advected

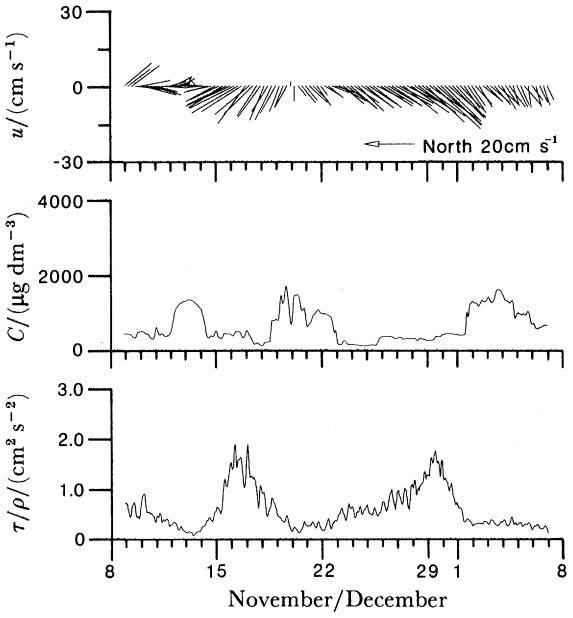

FIGURE 1. Three advected storm events, November 8–December 8, 1985. Speed and direction 5 m AB. Suspended sediment concentration based on light attenuation. Estimate of bed shear velocity from direct measures of kinetic energy.

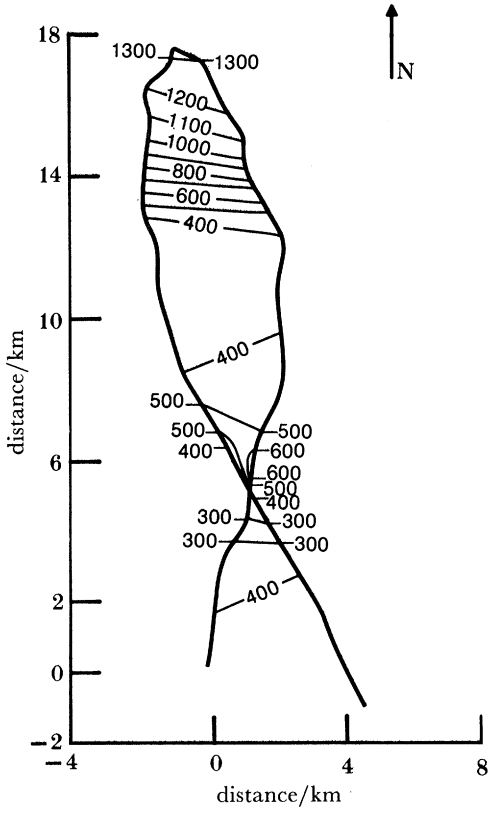

FIGURE 2. Inverse progressive vector diagram trace of suspended sediment field November 11–15.

pattern shows that this was not sediment suspended locally by erosion. Most sediment events were associated with rapid changes in flow velocity, direction and often temperature changes, all of which may indicate the arrival of different water masses. We refer to these types of suspended sediment episodes as 'advected events'.

Events on October 24 and June 15 are distinctly different from the advected events (figures 3 and 4). Photographs of the bed, before and after these events, show extensive bed

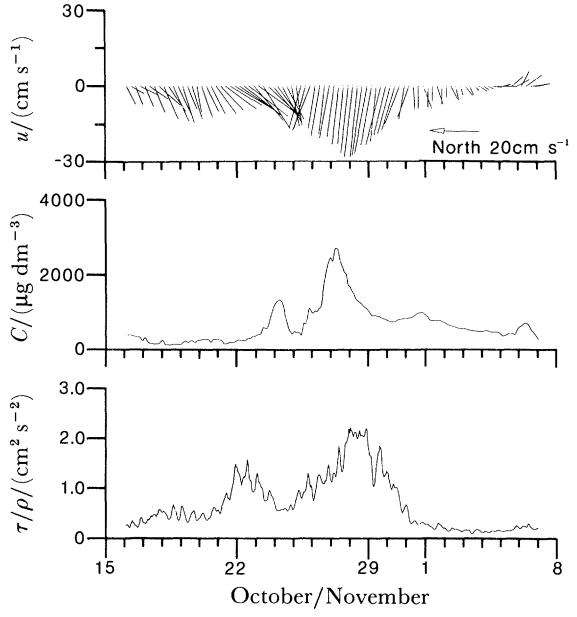

FIGURE 3. Local suspension event October 15–November 11, 1985. Speed and direction 5 m AB. Suspended sediment concentration based on light attenuation. Estimate of bed shear velocity from direct measures of kinetic energy.

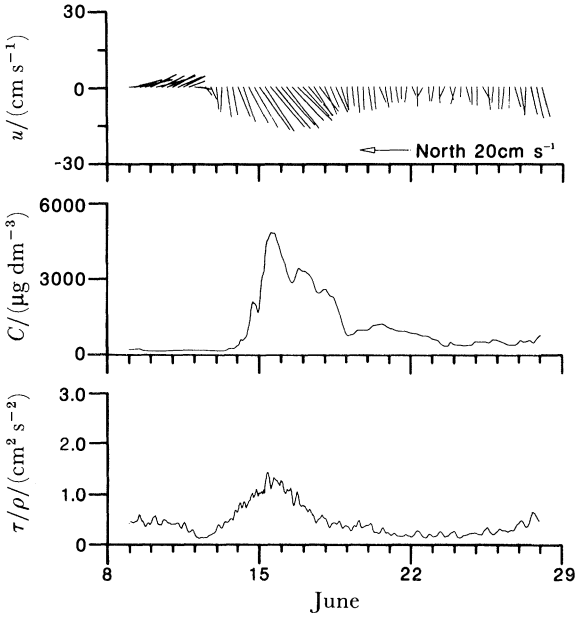

FIGURE 4. Local suspension event of June 8–29, 1986. Speed and direction 5 m AB. Suspended sediment concentration based on light attenuation. Estimate of bed shear velocity from direct measures of kinetic energy.

modification due to erosion and deposition. The peak sediment concentrations at 4 m AB were the largest observed and occurred just after the bed stress had passed through 1 dyn cm^{-2}†, approximately the critical erosion stress for cohesive sediments (Mehta *et al.* 1982). Peak sediment concentration leads the peak stress. After the erodible sediments were exhausted, the concentration at 4 m AB began to drop as the sediment was diluted by mixing throughout the turbulent bottom boundary layer. Both storms exhibited a small increase in suspended sediment followed by a large rise which lasts for about six hours. The first rise may have been the erosion of a 'fluff' layer. The second may have been deeper erosion of recently deposited, or biologically reworked, unconsolidated sediments. The ability of the current to erode sediment appears to be related to the age of the sediment and perhaps the direction of the previous currents under which the sediment was deposited (Gross & Williams 1990).

The October and June local erosion events lasted only about 7 days. As will be seen, the drop in concentration was due to vertical mixing and dilution, not to net deposition. However, the rapid clearing of the water column after both events was more likely due to advection of clear water into the area. The spatial dimension of the events was limited and of order 7 days $\times$ 20 cm $s^{-1} \approx 100$ km. On the one hand, the time history of an erosion event can be construed to represent the lagrangian local event. On the other hand, it must be recognized that eulerian measurements cannot follow the event and long-term decay of the sediment clouds. Deposition and clearing of storm induced sediment suspension can only be inferred by modelling the dynamics in a lagrangian sense, i.e. by assuming no advection of horizontal gradients.

Turbulent bottom boundary layer model

Further interpretation of the local erosion storm data requires a model of the sediment concentration profile. A full sediment-profile model based on near-bed measures of sediment concentration, velocity and stress provides estimates of total sediment eroded, depth of the resultant nepheloid layer, and its decay. Most sediment transport modelling efforts have been directed at investigating near-bed stress for prediction of erosion conditions (reviewed by Nowell 1983). For that problem eddy-diffusivity formulations valid within the logarithmic velocity region are adequate. The major problems that must be solved to understand HEBBLE storms relate to the height of mixing and entrainment into the upper water column. Simple eddy diffusivity models will not be adequate to describe the processes of entrainment and stratification limited boundary-layer growth. Although sediment induced stratification near the bed during erosion is of no importance, its inclusion in the outer layer model is important. The following turbulence model is based on the 2 and $2\frac{1}{2}$ level closure of Mellor & Yamada (1982).

For simplicity we begin with an one-dimensional eddy-diffusivity boundary-layer equation:

$$\frac{\partial \boldsymbol{U}}{\partial t} - \mathrm{i}f(\boldsymbol{U} - \boldsymbol{U}_{\mathrm{geos}}) = \frac{\partial}{\partial z} K \frac{\partial \boldsymbol{U}}{\partial z}, \tag{1}$$

where $\boldsymbol{U}$ is the complex vector velocity $U + \mathrm{i}V$, $\boldsymbol{U}_{\mathrm{geos}}$ is the outer geostrophic flow, K is the eddy diffusivity and f is the Coriolis frequency.

The closure method uses an eddy diffusivity obtained from the energy equation following

† 1 dyn = 10^5 N.

Mellor & Yamada (1974), Mellor & Yamada (1982), Lavelle & Mofjeld (1983) and Mofjeld & Lavelle (1984);

$$K = S_{\mathrm{m}}\, ql, \tag{2}$$

where q^2 is twice kinetic energy, $\overline{u'^2}+\overline{v'^2}+\overline{w'^2}=q^2$, and l is a depth dependent turbulence length scale. An energy estimate for use in the eddy diffusivity is obtained from the rate of change of energy equation:

$$\frac{\partial q^2/2}{\partial t} = \frac{\partial}{\partial z}\frac{S_q}{S_{\mathrm{m}}} K \frac{\partial q^2/2}{\partial z} + K\left|\frac{\partial \boldsymbol{U}}{\partial z}\right|^2 - \frac{q^3}{cl} + g'\,\overline{c'w'}. \tag{3}$$

The buoyancy energy sink due to suspended sediment, $g'\,\overline{c'w'}$, is modelled with the eddy diffusivity:

$$g'\,\overline{c'w'} = g' K\, \partial C_{\mathrm{v}}/\partial z, \tag{4}$$

where C_{v} is the volume concentration of particles and $g' = g(\rho_{\mathrm{sed}}-\rho_w)/\rho_w$ is reduced gravity. When time dependence and energy diffusion terms are retained this is the $2\frac{1}{2}$ level closure model. Energy diffusion may be required when stratification 'caps' the turbulent boundary layer. Inclusion of energy diffusion simulates entrainment processes in the outer layer. Mellor & Yamada (1982) provide estimates of the non-dimensional constants $[S_{\mathrm{m}}, c, S_q] = [0.4, 15, 0.2]$.

Alternatively, the level 2 model assumes the rate and diffusion terms are small compared with production, dissipation and buoyancy work, yielding

$$q^2 = S_{\mathrm{m}}\, cl^2\left\{\left|\frac{\partial \boldsymbol{U}}{\partial z}\right|^2 + g'\frac{\partial C_v}{\partial z}\right\}, \tag{5}$$

which results in

$$K = l^2\left\{\left|\frac{\partial \boldsymbol{U}}{\partial z}\right|^2 + g'\frac{\partial C_v}{\partial z}\right\}^{\frac{1}{2}}. \tag{6}$$

Mofjeld & Lavelle (1984) show that $S_m = c^{-\frac{1}{3}}$. Therefore the solution for $\boldsymbol{U}$ has no dependence on S_{m} or c.

The dissipation length scale l must be specified. The near-bed asymptotic solution of the logarithmic velocity profile requires $l = \kappa z$, for small z. Following Mofjeld & Lavelle (1984), Richards (1982), Weatherly & Martin (1978), Mellor & Yamada (1974) and Blackadar (1962) the outer layer condition that the eddy diffusivity should decrease is modelled with

$$l(z) = \kappa z/(1+\kappa z/L), \tag{7}$$

where the integral length scale L is given by

$$L = \gamma \int_{z_o}^{\delta} zq\,\mathrm{d}z \Big/ \int_{z_o}^{\delta} q\,\mathrm{d}z. \tag{8}$$

The parameter γ scales the depth of the turbulent boundary layer. Mofjeld & Lavelle (1984) found that the sparse oceanic data suggest $\gamma \approx 0.2$–0.3. As γ affects only the outer flow the boundary shear stress is insensitive to γ.

A common method used to modify a neutral eddy diffusivity, K_{n}, with near-bed stratification is,

$$K_{\mathrm{strat}} = K_{\mathrm{n}}/(1+\beta\zeta), \tag{9}$$

where $\zeta = z/L_{\mathrm{m}}$ and the Monin Obukov length scale, $L_{\mathrm{m}} = u_*^3/\kappa g'\,\overline{c'w'_o}$, is derived from the

near-bed buoyancy flux work and energy dissipation (Taylor & Dyer 1977; Smith & McLean 1977; McLean 1985). The above stratification correction and the form of l in equation (7) can be manipulated to yield

$$K \approx S_{\mathrm{m}}\, q\, \kappa z \Big/ \left(1+\beta \frac{z}{L_{\mathrm{m}}}+\frac{z}{L/\kappa}\right). \tag{10}$$

If L_{m} is smaller than L/κ then the solution is not dependent on the value of γ. Kitaigorodskii (1988) derives expressions for the scale height ratios of Ekman depth and buoyancy depth and concludes that Ekman depth (which is scaled by γ) is often the larger, and therefore less influential, scale. Stratification will have the effect of lowering the value of γ accounting for γ values of approximately 0.1 found in atmospheric work, where neutral stratification is quite rare and difficult to confirm (Mofjeld & Lavelle 1984).

The lower boundary condition for the velocity profile is a specified level of no motion, z_o.

$$\boldsymbol{U}(z_o) = 0. \tag{11}$$

The upper condition on the highest grid point, z_n, is a no stress condition implemented on the velocity using:

$$\partial \boldsymbol{U}(z_{\mathrm{n}})/\partial t - \mathrm{i}f(\boldsymbol{U}(z_{\mathrm{n}}) - \boldsymbol{U}_{\mathrm{geos}}) = 0. \tag{12}$$

The outer forcing for such a model is usually taken as a prescribed time variation of $\boldsymbol{U}_{\mathrm{geos}}$. Our measurements did not extend above the boundary layer and did not provide direct measures of $\boldsymbol{U}_{\mathrm{geos}}$. The velocity measured by the highest BASS sensor at 5 m AB was used as the forcing function by solving for $\boldsymbol{U}_{\mathrm{geos}}$, which satisfied

$$\frac{\partial \boldsymbol{U}_5}{\partial t} - \mathrm{i}f(U_5 - U_{\mathrm{geos}}) = \frac{\partial}{\partial z} K \frac{\partial \boldsymbol{U}}{\partial z}\bigg|_{z=5} \tag{13}$$

The initial starting point was always chosen as a period of low flow, ($\boldsymbol{U}_{5\mathrm{m\,AB}} < 5$ cm s^{-1}), several days before the period of interest. The iterative solution to the above equation for $\boldsymbol{U}_{\mathrm{geos}}$ rapidly converges at initialization and remains relatively stable across large changes in forcing. The geostrophic velocity solution is sensitive to accelerations. Therefore the forcing time series at 5 m AB must be carefully interpolated to avoid spurious accelerations in the geostrophic velocity. The simulated velocity near 5 m AB will not reflect such deviations in the geostrophic velocity but the kinetic energy can increase in the outer layer due to rapid accelerations. The modelled geostrophic velocity is actually a combination of outer flow velocity and baroclinic pressure gradients. When a sediment induced pycnocline is present the difference from an outer layer velocity will become significant. This technique, based on near-bed velocity forcing, reproduces the near-bed stress more accurately than a model forced by outer velocity measurements.

Suspended sediment profiles are modelled by using the eddy diffusivity derived above with the mass conservation equation:

$$\frac{\partial C_{\mathrm{v}}}{\partial t} = w_{\mathrm{f}} \frac{\partial C_{\mathrm{v}}}{\partial z} + \frac{\partial}{\partial z} K(z,t) \frac{\partial C_{\mathrm{v}}}{\partial z}, \tag{14}$$

where C_{v} is the volume concentration of particles of fall velocity w_{f}. The upper boundary condition is zero mass-flux. The lower condition will be a flux condition dependent on the erodibility of the bed. The observed sediment concentration during storms peaks quickly. The total in suspension does not represent more than a few millimeters of erosion. A limit on the

total erosion must be used. This is naturally modelled by assuming that the surface consists of about 1 mm of easily eroded silt and clay, with a critical erosion shear stress of *ca.* 1 dyn cm^{-2}. Below the erodible phase there is a layer of consolidated sediment with a much higher yield strength, $\tau_{crit} > 10$ dyn cm^{-2}. This value for critical shear stress is close to the observed critical shear stress value of figures 3 and 4 and agrees with work on cohesive sediments (Lavelle *et al.* 1984; Mehta *et al.* 1982). Because complete erosion occurs relatively quickly the precise formulation of the erosion condition does not affect the development of the suspended sediment concentration profile. The rate of erosion is taken to be a simple excess stress formulation:

$$(\partial C_v(z_1)/\partial t)_{erosion} = w_e C_{bed} S/S_0 z_1, \tag{15}$$

where the change in concentration of the bottom bin at z_1 is the mass flux from the bed per the depth of the bottom bin. $S = (\tau - \tau_{crit})/\tau_{crit}$ is the non-dimensional excess shear stress. The rate of flux is scaled with an erosion velocity, $w_e/S_0 = \delta_e/t_e$, defined by the timescale, t_e, needed to erode the bed layer of depth, δ_e, at an excess shear stress of $S_0 \approx 0.10$. The data of figure 3 indicate the timescale is about 6 hours. Deposition continuously occurs through the fall velocity term of equation (14). As deposition is small compared with erosion during periods of net erosion no changes are made to the erosion–deposition equation except through the value of excess shear stress, S.

The model will calculate the concentration profiles for several particle size ranges. Three size ranges were chosen based on the results of the remote optical settling tube deployment at the start of the long HEBBLE deployment (McCave & Gross 1990). Two main modes, diameter 5 μm, fall velocity 0.0004 cm s^{-1} and diameter 42 μm, fall velocity 0.012 cm s^{-1} are separated by a median plateau of diameter 14 μm, fall velocity 0.002 cm s^{-1}. The storm of June 15 1986 had a maximum suspended sediment concentration of 5500 μg dm^{-3} at 4 m AB. The depth of erosion of the bed was adjusted to give approximately this level. When the total density of the particles in the erodible bed is a porous 0.2 g cm^{-3}, the erosion depth is found to be *ca.* 0.5 mm. The different particle-size mass-concentration profiles will be summed and the result will be used for the stratification term of equation (3) or (6).

The model is solved on a 150-point log–linear spaced grid using implicit time stepping by tridiagonal matrix inversion. The velocity, energy and then concentration profiles are staggered in time to enable separation and the use of the tridiagonal technique.

Model results

The storm of June 15 is modelled using the velocity data from 5 m AB (figure 4) and a constant bed roughness scale, $z_o = 0.5$ cm. Several variations of the model will be compared and discussed. The level two model, using the steady-energy equations (6)–(8), will be run with stratification and the effect of the parameter $\gamma = 0.2$ or 0.3 will be examined. The level $2\frac{1}{2}$ model using time dependent energy equations with diffusion and stratification, equations (3), (7) and (8), will be demonstrated. Features of the June 15 storm that differ from the October 24 storm will be compared.

Stratified steady energy equation

The general features of the sediment transport storm of June 15 are recreated by model runs (figures 5 and 6). The time series of sediment concentration at 4 m AB leads the peak stress. This is, of course, a direct consequence of the limited erosion depth model and the critical erosion

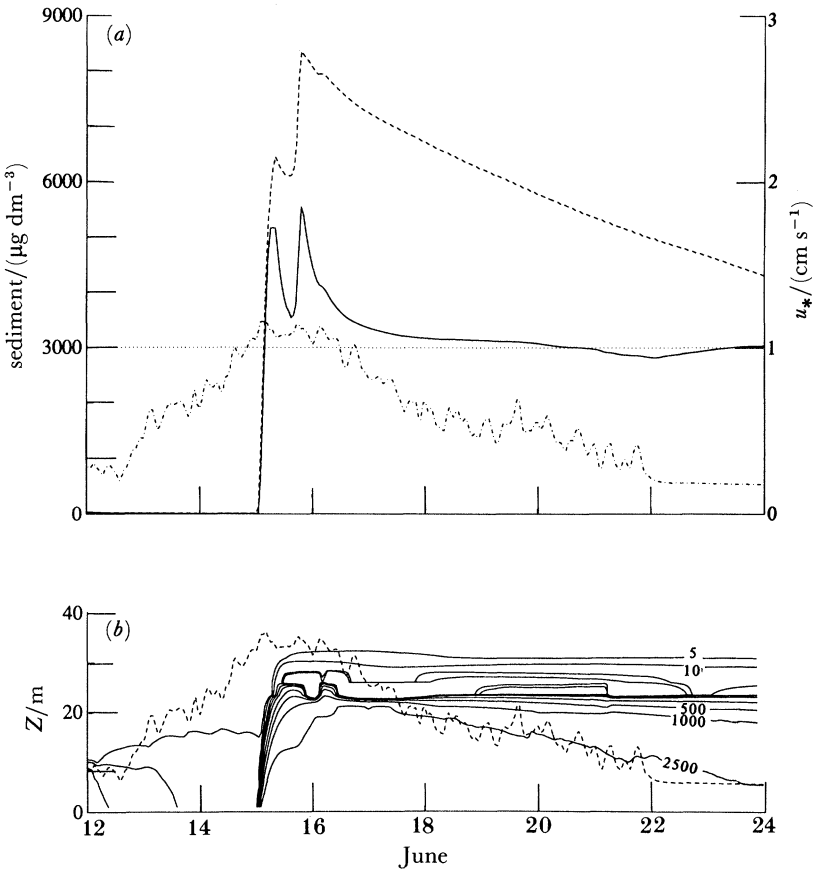

FIGURE 5. Steady stratified model of q^2 with $\gamma = 0.2$. Forcing for the model is from velocity of figure 7. (*a*) ——, suspended sediment concentration at 4 m AB; – – –, total sediment in suspension; —·—·, shear stress velocity scale u_*; ...., critical shear stress velocity scale. (*b*) ——, contours of total suspended sediment concentration; – – – –, scale height of planetary boundary layer, $\kappa u_*/f$. Values indicated are in μg dm^{-3}.

stress used. The rate of erosion, proportional to excess shear S, is barely able to stay ahead of the rate of deposition of large particles. The total mass in suspension, therefore, fluctuates with changes in excess shear. But, the source is largely cut off and the total in suspension remains relatively constant. The concentration at 4 m AB drops rapidly due to dilution. The contour plot of concentration indicates that such a sharp decline in suspended concentration would not be observed higher in the water column.

Variation of γ has a small effect on the near-bed stress. Larger γ decreases the eddy diffusivity length scale which, as U(5 m AB) is fixed, increases the stress scale, u_*. This is a small effect which becomes amplified in the excess shear stress or erosion rate. For $\gamma = 0.3$ the large particles are held in suspension and total mass is less variable than for the case $\gamma = 0.2$ (figure 6).

The greatest effect of γ should be the outer boundary-layer scale height. As expected from equation (10), γ has little effect on the structure of the eddy diffusivity when stratification is present. The $\gamma = 0.3$ case established a higher level for the pycnocline in the first few hours of erosion before the stratification effect became dominant. Sediment diffuses up to the level where $|\partial U/\partial z|^2 = -g' \partial C/\partial z$ above which equation (5) then gives zero kinetic energy. A possibility of negative energy is an unrealistic feature of this closure method (Hassid & Galperin

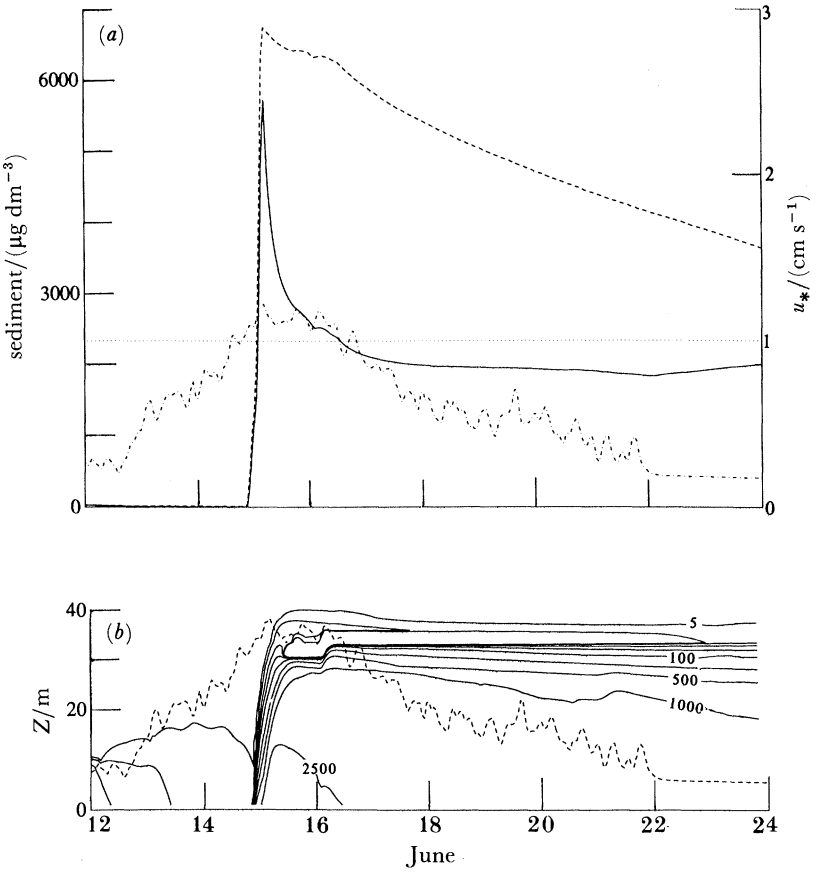

FIGURE 6. Steady stratified model of q^2 with $\gamma = 0.3$. See legend of figure 5.

1983). Negative values of energy are set to zero and the model forms a pycnocline, which remains at this level. Further mixing below this level intensifies the gradient at the suspended sediment pycnocline. This model provides no mechanism by which the nepheloid layer might deepen by entrainment. Before such a strongly stratified region develops, internal waves would generate and break causing both energy production and mixing. This suggests that including a term for entrainment of non-turbulent clear water into the turbulent boundary-layer is necessary.

Time-dependent energy equation with diffusion

Inclusion of diffusion of energy raises the order of the closure scheme to Mellor & Yamada's level $2\frac{1}{2}$. Time dependence in the energy equation is necessary if production and dissipation become unbalanced as often occurs under strong accelerations. Richards (1982) showed that small phase shifts in the energy and stress relative to velocity shear can occur in planetary boundary layers driven by strong tidal oscillations. The oscillatory component of flow during HEBBLE storms is small compared with the mean current, and rapid accelerations are rare. However, as the numerical solution method is virtually identical whether or not time dependence is included, the model retains the rate term of equation (3).

The addition of time dependence in the energy equation causes the maximum stress near the bed to be a few percent greater. During accelerating flows, production leads dissipation with the imbalance resulting in a slightly greater predicted stress.

Stratification suppresses the depth of the nepheloid layer (figure 7). Diffusion of kinetic energy allows a small mass and energy flux out of the turbulent boundary layer. The layer slowly thickens. For the June 15 storm the outer forcing is barely competent to erode the bed and turbulence decreases shortly after the full turbulent boundary layer is formed. Even so, the small levels of turbulence present are capable of raising the top of the nepheloid layer after the erosion event is over. At very low turbulence levels the mid-sized particles are able to settle resulting in an increase of sediment concentration below 10 m.

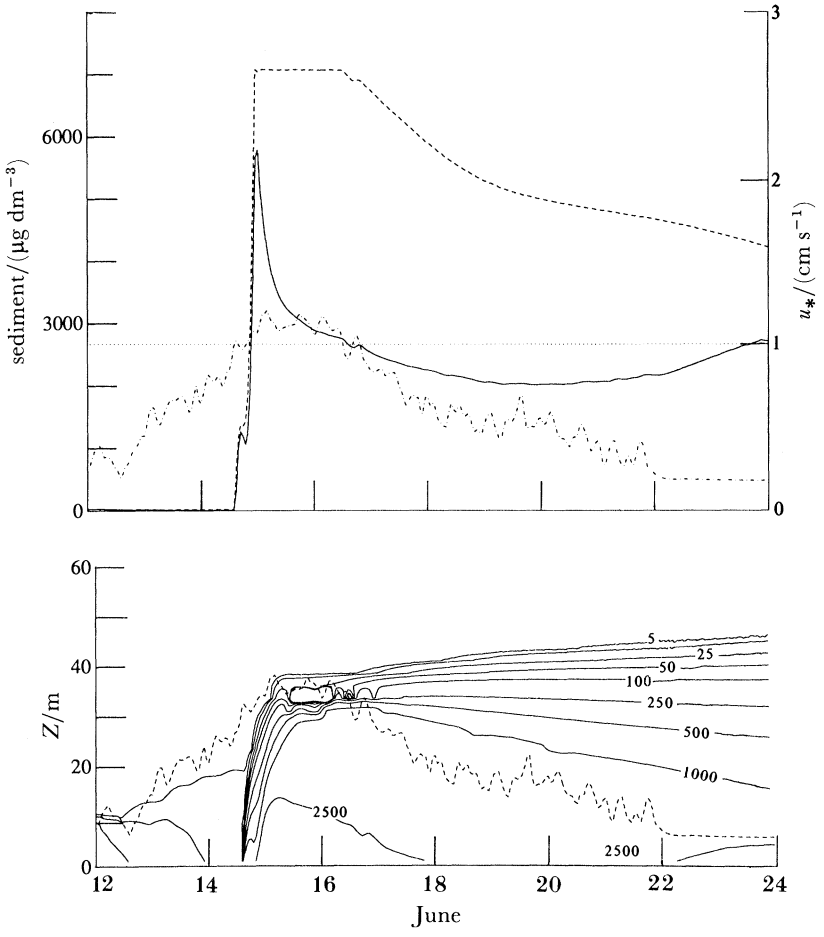

FIGURE 7. Time dependent energy with diffusion and stratification, $\gamma = 0.3$. See legend of figure 5.

The storm of October 24 differed from the June storm in two significant points.

1. The October storm currents reached larger magnitude before decreasing. The maximum u_* was almost 50% greater. Therefore, a thicker turbulent boundary layer is expected in the absence of stratification.

2. The amount of sediment eroded by the October storm was apparently less. The October storm maximum suspended load at 4 m AB was *ca.* 2700 μg dm^{-3}, about half the maximum of the June storm of *ca.* 5500 μg dm^{-3}. There would have been less stratification effect.

Together, these two factors imply that the inclusion of diffusion, when modelling the October storm, will thicken the nepheloid layer more than was observed from the model runs

of the June storm. The model run of the October storm with stratification and diffusion indicates a more complicated suspended sediment pattern (figure 8). Higher levels of turbulence during the October event are able to mix particles quickly in the vertical and the stratification front is weakly formed at a higher level. The structure of the outer regions is due to the rapid fall of 45 μm particles when stress begins to decay. The contribution of all three size particles is equivalent when the stress is high and the boundary-layer height is limited by growth rate (figure 9). The largest particles deposit when the stress begins to decline. Deepening of the nepheloid layer is due to mixing of the finest particles.

An interesting paradox is revealed in comparisons of the two storms. The apparently more intense storm of June created a thinner nepheloid layer than the weaker storm of October.

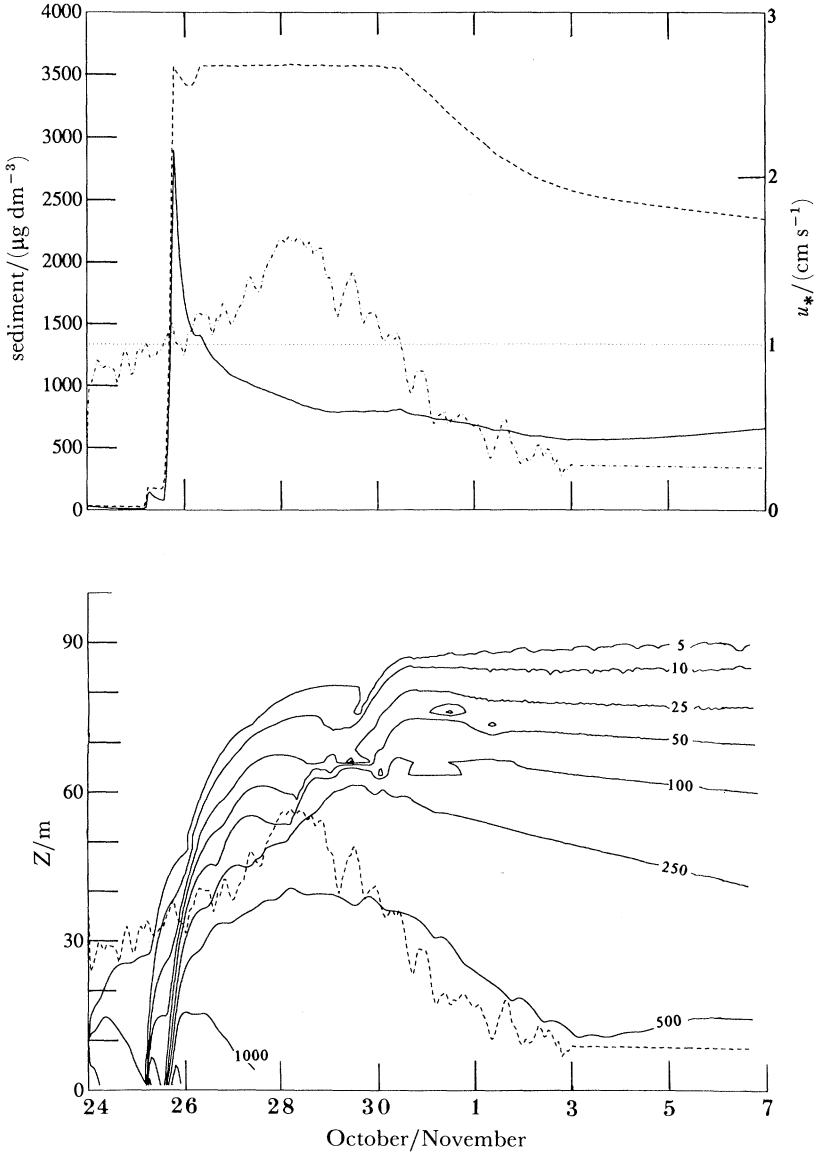

FIGURE 8. Time-dependent energy with diffusion and stratification, $\gamma = 0.3$. October 27 storm demonstrating the two effects of a smaller source and greater shear stress than the June storm of figure 7. See legend of figure 5.

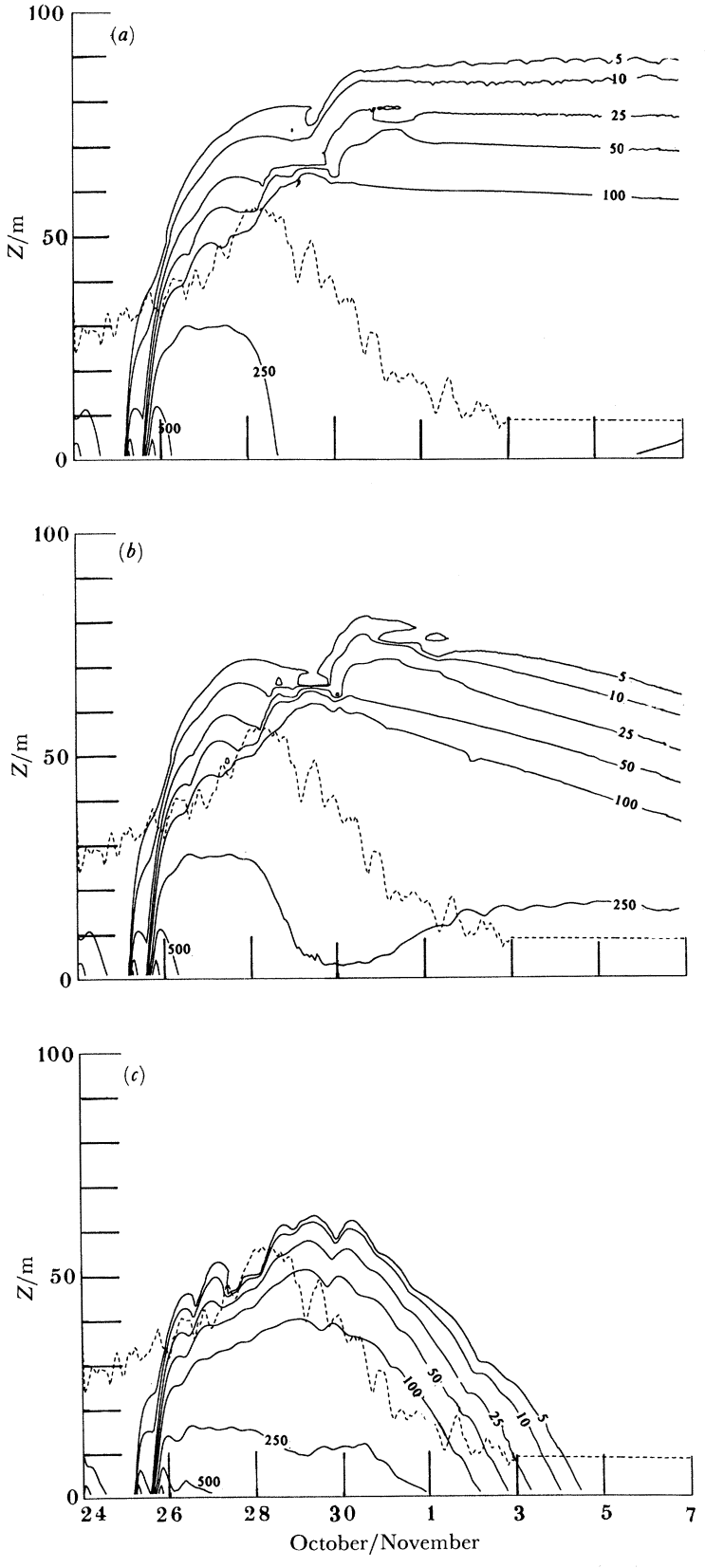

FIGURE 9. Contours of suspended sediment of the three size classes, (*a*) 5 μm, (*b*) 14 μm and (*c*) 42 μm. ----, Scale height of planetary boundary layer, $\kappa u_*/f$.

PHILOSOPHICAL TRANSACTIONS OF THE ROYAL SOCIETY A MATHEMATICAL, PHYSICAL & ENGINEERING SCIENCES

Clearing rate, due to fall velocity, of the near-bed nepheloid layer is proportional to depth. Sediments suspended by the June storm would clear more quickly. The weaker October storm would result in a more persistent contribution to the world nepheloid layer.

Conclusions

Data obtained during the HEBBLE long deployment have demonstrated that occasional high energy erosive events occur along the Nova Scotian Rise, which suspend appreciable amounts of sediment. Local suspension events are rare, yet such events seem to suspend enough sediment to account for the presence of advected suspended sediment clouds in the area. Model simulations imply that vertical mixing is limited by sediment stratification during the most intense of these storms. A suspended sediment pycnocline is formed from 30 to 80 m above the bed. Two local erosion storms were observed that differed in the total sediment eroded and maximum shear stress. The depth of the modelled nepheloid layer increased with either greater bed stress or a smaller suspended load. Greater stress can break down the pycnocline resulting in a deeper nepheloid layer. Weaker stratification allows greater vertical mixing and hence a deeper turbulent layer. The two observed storms differed in these two aspects by enough to predict nepheloid layers differing in thickness by a factor of two. The benthic nepheloid layer is variable in time due to the episodic nature of the forcing and is variable in structure due to maximum bed stress and total sediment eroded.

The effect of stratification by eroded sediment was shown to reduce the dependence of the model on closure assumptions in the outer region. An energy diffusion closure is required to overcome an unrealistically sharp pycnocline. Without an energy diffusion term, stratification will prevent entrainment of clear water across the pycnocline. With diffusion and sufficiently large stress the pycnocline can be eroded, giving a nepheloid layer up to 90 m deep.

A principle conclusion resulting from this study is that future experiments must include measurements at depths of 20–100 m of stress, energy and suspended sediment. The rate of entrainment and eventual depth of the nepheloid layer is dependent on the coefficient scaling the energy diffusion. To investigate this parameter measures of energy production, dissipation and gradient must be made where all three are important, i.e. above the logarithmic region. Measures of the suspended sediment in the region of the sediment pycnocline will elucidate the mixing process and reveal the total sediment load more accurately than single point measures near the bed in the fully mixed region.

This work was funded by ONR contract N00014-88-K0028 and NSF contract OCE-8609806.

References

Blackadar, A. K. 1962 The vertical distribution of wind and turbulent exchange in a neutral atmosphere. *J. geophys. Res.* **67**, 3095–3120.

Gross, T. F., Williams, A. J. & Grant, W. D. 1986 Long-term in situ calculations of kinetic energy and Reynolds stress in a deep sea boundary layer. *J. geophys. Res.* **91**, 8461–8469.

Gross, T. F., Williams, A. J. & Nowell, A. R. M. 1988 A deep-sea sediment transport storm. *Nature, Lond.* **331**, 518–521.

Gross, T. F. & Williams, A. J. 1990 Characterization of deep sea storms. *Deep Sea Res.* (In the press.)

Hassid, S. & Galperin, B. 1983 A turbulent energy model for geophysical flows. *Bound.-Layer Meteor.* **26**, 397–412.

Hollister, C. D. & McCave, I. N. 1984 Sedimentation under deep-sea storms. *Nature, Lond.* **309**, 220–225.
Kitaigorodskii, S. A. 1988 A note on similarity theory for atmospheric boundary layers in the presence of background stable stratification. *Tellus* A **40**, 434–438.
Lavelle, J. W. & Mofjeld, H. O. 1983 Effects of time-varying viscosity on oscillatory turbulent channel flow. *J. geophys. Res.* **88**, 7607–7616.
Lavelle, J. W., Mofjeld, H. D. & Baker, E. T. 1984 An *in situ* erosion rate for a fine-grained marine sediment. *J. geophys. Res.* **89**, 6543–6552.
McCave, I. N. & Gross, T. F. 1990 *In situ* measurements of particle settling velocity in the deep sea. *Deep Sea Res.* (In the press.)
McLean, S. R. 1985 Theoretical modeling of deep ocean sediment transport. *Mar. Geol.* **66**, 243–265.
Mehta, A. J., Parchure, T. M., Dixit, J. G. & Ariathurai, R. 1982 Resuspension potential of deposited cohesive sediment beds. In *Estuarine comparisons* (ed. V. Kennedy), pp. 591–609. New York: Academic Press.
Mellor, G. L. & Yamada, T. 1974 A hierarchy of turbulence closure models for planetary boundary layers. *J. atmos. Sci.* **31**, 1791–1803.
Mellor, G. L. & Yamada, T. 1982 Development of a turbulence closure model for geophysical fluid problems. *Rev. Geophys. Space Phys.* **20**, 851–875.
Mofjeld, H. O. & Lavelle, J. W. 1984 Setting the length scale in a second-order closure model of the bottom boundary layer. *J. phys. Oceanogr.* **14**, 833–839.
Nowell, A. R. M., Hollister, C. D. & Jumars, P. A. 1982 High energy benthic boundary layer experiment: HEBBLE. *Eos, Wash.* **63**, 594–595.
Nowell, A. R. M. 1983 The benthic boundary layer and sediment transport. *Rev. Geophys. Space Phys.* **21**, 1181–1192.
Richards, K. J. 1982 Modeling the benthic boundary layer. *J. phys. Oceanogr.* **12**, 428–439.
Smith, J. D. & McLean, S. R. 1977 Boundary layer adjustments to bottom topography and suspended sediment. In *Bottom turbulence* (ed. J. Nihoul), pp. 123–151. Amsterdam: Elsevier.
Taylor, P. A. & Dyer, K. R. 1977 Theoretical model of flow near the bed and their implications for sediment transport. In *The sea* (ed. E. D. Goldberg), vol. 6, pp. 579–601. New York: Wiley-Interscience.
Thistle, D., Yingst, J. Y. & Fauchald, K. 1985 A deep-sea benthic community exposed to strong near bottom currents on the Scotian Rise. *Mar. Geol.* **66**, 91–112.
Weatherly, G. L. & Martin, P. J. 1978 On the structure and dynamics of the oceanic bottom boundary layer. *J. phys. Oceanogr.* **8**, 557–570.
Williams, A. J., Tochko, J. S., Koehler, R. L., Grant, W. D., Gross, T. F. & Dunn, C. V. R. 1987 Measurement of turbulence in the oceanic bottom boundary layer with an Acoustic Current Meter Array. *J. atmos. Ocean. Technol.* **4**, 312–327.

PHILOSOPHICAL TRANSACTIONS OF THE ROYAL SOCIETY A MATHEMATICAL, PHYSICAL & ENGINEERING SCIENCES